# Redox-Active vs Redox-Innocent: A Comparison of Uranium Complexes Containing Diamine Ligands

Scott A. Pattenaude,[†] Kimberly C. Mullane,[‡] Eric J. Schelter,[‡] Maryline G. Ferrier,[§] Benjamin W. Stein,[§] Sharon E. Bone,[§] Juan S. Lezama Pacheco,[⊥] Stosh A. Kozimor,[§] Phillip E. Fanwick,[†] Matthias Zeller,[†,∥] and Suzanne C. Bart*[,†]

[†]H. C. Brown Laboratory, Department of Chemistry, Purdue University, West Lafayette, Indiana 47907, United States

[‡]P. Roy and Diana T. Vagelos Laboratories, Department of Chemistry, University of Pennsylvania, Philadelphia, Pennsylvania 19104, United States

[§]Los Alamos National Laboratory, Los Alamos, New Mexico 87545, United States

[∥]Department of Chemistry, Youngstown State University, Youngstown, Ohio 44555, United States

[⊥]Department of Earth System Science, Stanford University, Stanford, California 94305, United States

**ABSTRACT:** Uranium complexes ($^{Mes}$DAE)$_2$U(THF) (**1-DAE**) and Cp$_2$U($^{Mes}$DAE) (**2-DAE**) ($^{Mes}$DAE = [ArN-CH$_2$CH$_2$-NAr]; Ar = 2,4,6-trimethylphenyl (Mes)), bearing redox-innocent diamide ligands, have been synthesized and characterized for a full comparison with previously published, redox-active diimine complexes, ($^{Mes}$DAB$^{Me}$)$_2$U(THF) (**1-DAB**) and Cp$_2$U($^{Mes}$DAB$^{Me}$) (**2-DAB**) ($^{Mes}$DAB$^{Me}$ = [ArN=C(Me)C(Me)=NAr]; Ar = Mes). These redox-innocent analogues maintain an analogous steric environment to their redox-active ligand counterparts to facilitate a study aimed at determining the differing electronic behavior around the uranium center. Structural analysis by X-ray crystallography showed **1-DAE** and **2-DAE** have a structural environment very similar to **1-DAB** and **2-DAB**, respectively. The main difference occurs with coordination of the ene-backbone to the uranium center in the latter species. Electronic absorption spectroscopy reveals these new DAE complexes are nearly identical to each other. X-ray absorption spectroscopy suggests all four species contain +4 uranium ions. The data also indicates that there is an electronic difference between the bis(diamide)-THF uranium complexes as opposed to those that only contain one diamide and two cyclopentadienyl rings. Finally, magnetic measurements reveal that all complexes display temperature-dependent behavior consistent with uranium(IV) ions that do not include ligand radicals. Overall, this study determines that there is no significant bonding difference between the redox-innocent and redox-active ligand frameworks on uranium. Furthermore, there are no data to suggest covalent bonding character using the latter ligand framework on uranium, despite what is known for transition metals.

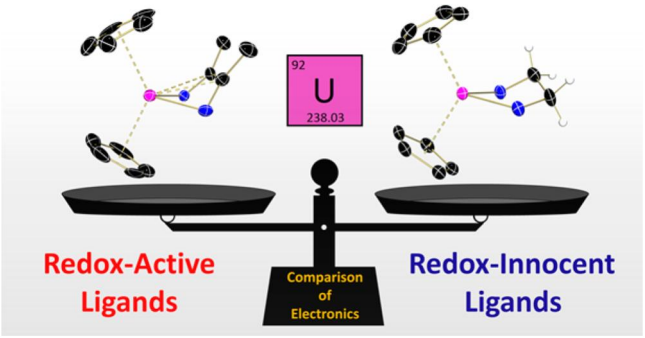


## ■ INTRODUCTION

Redox-active ligands, those that participate in redox chemistry with a metal rather than existing as spectators, have recently risen to the forefront of inorganic and organometallic chemistry.[1−10] These ligands serve as electron reservoirs that work in concert with metal centers to mediate multielectron reactions that would not otherwise be possible.[5,6] Along with providing this unique capability to metals that are typically redox-restricted, these ligands also impart additional complexity to the electronic structures of coordination complexes.[11] The origin of this complexity lies in the very root of their functionality, energetically accessible $\pi^*$ orbitals that can accept electron density, or supply electron density subsequent to filling. Pioneering studies have demonstrated the utility of combining multiple analytical tools to elucidate ground state electronic structures including NMR spectroscopy, X-ray crystallography, X-ray absorption spectroscopy, Mössbauer spectroscopy (where appropriate), computational modeling, and magnetic studies.[12−16]

In recent years, our group[17−22] and others[23−26] have extended these studies to the elements of the f-block, and more specifically uranium, bringing additional complexity to the already electronically diverse actinide elements. By utilizing the above-mentioned techniques, uranium complexes bearing redox-active ligands in a variety of ground states have been established. These highly reduced, electron-rich uranium species readily perform multielectron transfer

chemistry,[20,27−29] showing that in appropriate chemical environments, a metal that typically only does one-electron chemistry, like uranium, can behave like a late transition metal. In contrast, oxidation of redox-active salen ligands has also been reported. Work from Leznoff and Storr highlights the oxidation of neutral salen ligand derivatives of uranyl, which have been isolated and characterized to contain localized salen ligand radicals.[30] Similarly, electrochemical oxidation of a tetrathiafulvalene-salphen actinide complex produced the corresponding radical cation species in solution, which was proposed to be stable due to delocalization over the extended $\pi$-system of the complex as determined by computation.[10]

Studies of first row transition metal species bearing redox-active ligands conclude that electrons are highly delocalized over the entirety of the complex.[15,31−33] This is in part due to the energy match and orbital overlap between the ligand $\pi^*$-orbitals and the metal d-orbitals, generating species that are highly covalent. It is well established that the actinides' valence 5f-orbitals do not participate in covalent bonding equivalently to the valence d-orbitals associated with the transition metals, in part due to their more limited radial extension. Thus, there remains the question as to whether redox-active ligands impart additional covalent character to actinide complexes, given the energetically similar metal and ligand orbitals.

In 2011, we reported a full electronic structure study of uranium complexes bearing redox-active diazabutadiene ligands, namely, $(^{Mes}DAB^{Me})_2U(THF)$ (**1-DAB**) and $Cp_2U(^{Mes}DAB^{Me})$ (**2-DAB**) ($^{Mes}DAB^{Me}$ = [ArN=C(Me)C(Me)=NAr], where Ar = 2,4,6-trimethylphenyl (Mes)).[34] As determined by a combined spectroscopic, structural, and computational study, these species feature the doubly reduced ene-diamide ligands, $[^{Mes}DAB^{Me}]^{2-}$, along with uranium(IV) ions. An interesting structural highlight was the association of the C−C $\pi$-bond of the reduced ene-diamide ligand backbone to the uranium center, which has recently also been observed for uranium[35] and the lanthanides with similar ligand frameworks.[36−39] At the time, variable temperature magnetic data that were collected for these species gave anomalous results with values that would not be expected for uranium(IV) species. As an extension of this study, we proposed that generating the redox-innocent version of these complexes would provide insight into this unusual magnetic behavior and perhaps be instructive toward understanding potential covalent behavior with actinides. Herein we present our work on the redox innocent analogues to **1-DAB** and **2-DAB**, $(^{Mes}DAE)_2U(THF)$ (**1-DAE**) and $Cp_2U(^{Mes}DAE)$ (**2-DAE**), which are simple uranium(IV) complexes with diamide chelates ($^{Mes}DAE$ = $[ArN\text{-}CH_2CH_2\text{-}NAr]^{2-}$, where Ar = Mes) (Figure 1). To preserve the sterics of the original $^{Mes}DAB^{Me}$ system, the diamine ligand was synthesized with the bulky mesityl substituents on the nitrogen atoms. Once again, a study that combines spectroscopic, structural, and magnetic measurements was undertaken to directly compare to the redox-active ligand system.

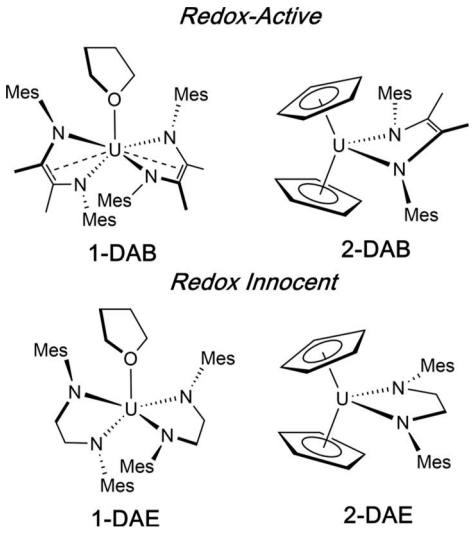


**Figure 1.** Uranium complexes featured in this study.

## ■ EXPERIMENTAL SECTION

**General Considerations.** *Caution: U-238 is a weak α-emitter with a half-life of $t_{1/2} = 4 \times 10^9$ years. This material should only be handled in a laboratory equipped with proper detection equipment.* All air- and moisture-sensitive manipulations were performed using standard Schlenk techniques or in an MBraun inert atmosphere drybox with an atmosphere of purified nitrogen. The MBraun drybox was equipped with a cold well designed for freezing samples in liquid nitrogen as well as two −35 °C freezers for cooling samples and crystallizations. Solvents for sensitive manipulations were dried and deoxygenated using literature procedures with a Seca solvent purification system.[40] Benzene-$d_6$ and chloroform-*d* were purchased from Cambridge Isotope Laboratories. Deuterated solvents were dried with molecular sieves and degassed by three freeze−pump−thaw cycles. *N,N′*-Dimesitylethane-1,2-diamine dihydrochloride,[41] $KCH_2Ph$,[42] and $UCl_4$[43] were prepared according to literature procedures. NaCp solution (2.0 M in THF) was purchased from Sigma-Aldrich and used as received.

$^1H$ NMR spectra were recorded on a Varian Inova 300 spectrometer at 299.992 MHz. All chemical shifts are reported relative to the peak for $SiMe_4$, using $^1H$ (residual) chemical shifts of the solvent as a secondary standard. The spectra for paramagnetic molecules were obtained by using an acquisition time of 0.5 s; thus, the peak widths reported have an error of ±2 Hz. For paramagnetic molecules, the $^1H$ NMR data are reported with the chemical shift, followed by the peak width at half height in Hertz, the integration value, and, where possible, the peak assignment. Elemental analyses were performed by Complete Analysis Laboratories, Inc., Parsippany, New Jersey. Electronic absorption measurements were recorded at 294 K in THF in sealed 1 cm quartz cuvettes with a Jasco V-6700 spectrophotometer. Infrared spectra were recorded using a PerkinElmer FT-IR spectrum RX I spectrometer. Samples were made by crushing the solids, mixing with dry KBr, and pressing into a pellet.

Single crystals of **1-DAE** or **2-DAE** for X-ray diffraction were coated with poly(isobutene) oil in a glovebox and quickly transferred to the goniometer head of either a Bruker AXS APEXII CCD diffractometer (**1-DAE**) or a Nonius KappaCCD diffractometer (**2-DAE**). Preliminary examination and data collection were performed with Mo $K_\alpha$ radiation ($\lambda$ = 0.71073 Å). See the Supporting Information for details on single crystal structure determinations.

Solid-state magnetic data were collected using a Quantum Design Multi-Property Measurement system (MPMS-7) warmed from 2−300 K and cooled from 300−2 K at 1 T and at 2 K from 0−7 T. Drinking straws were used to house the samples for measurement and were dried under a dynamic vacuum overnight before use in an inert atmosphere ($N_2$) drybox. While empty, the straws were crimped using a hot pair of tweezers to melt the straw together. The samples were added directly into the crimped straw and were massed to the nearest 0.1 mg using a calibrated and leveled Mettler-Toledo AL-204 analytical balance. Approximately 10.0 mg of quartz wool was added to the straw above the sample to hold it in place. The straw was then crimped above the sample and quartz wool with hot tweezers to complete the seal. The samples, contained in the sealed drinking straws for measurement, were transferred to the MPMS under inert atmosphere and immediately loaded into the inert atmosphere of the measurement chamber with three evacuation/purge cycles. Corrections for the

intrinsic diamagnetism of the samples were made using Pascal's constants.[44]

Samples of $Cs_2UO_2Cl_4$, **1-DAE**, **2-DAE**, **1-DAB**, and **2-DAB** were analyzed by U $L_3$-edge X-ray absorption spectroscopy measurements. Samples were prepared under an argon atmosphere. The samples were diluted with boron nitride (BN), which was dried at elevated temperature (200 °C) under a vacuum ($10^{-3}$ Torr) for 24 h prior to use. A mixture of the analyte and BN were weighed out, such that the edge jump for the absorbing atom was calculated to be at 1 absorption length in transmission (~30–50 mg of sample and 50–30 mg of BN). Samples were ground using a Wig-L-Bug, a Teflon bead, and a polycarbonate capsule. The finely ground powders were pressed as a pellet into a slotted aluminum sample holder equipped with Kapton windows (1 mil); one was fixed with super glue, and the other was Kapton tape. This primary holder was nested within a secondary aluminum holder equipped with Kapton (2 mil) windows that were sealed with indium wire. The samples were sealed in Mylar bags and shipped to the Stanford Synchrotron Radiation Lightsource (SSRL). Once unpackaged, the samples were immediately attached to the coldfinger of a liquid $N_2$ cryostat and quickly evacuated ($10^{-7}$ Torr). The cryostat was attached to the beamline 11-2 XAFS rail (SSRL), which was equipped with three ionization chambers through which nitrogen gas was continually flowed. One chamber (10 cm) was positioned before the cryostat to monitor the incident radiation ($I_0$). The second chamber (30 cm) was positioned after the cryostat so that sample transmission ($I_1$) could be evaluated against $I_0$ and so that the absorption coefficient ($\mu$) could be calculated as $\ln(I_0/I_1)$. The third chamber ($I_2$; 30 cm) was positioned downstream from $I_1$ so that the XANES spectrum of a calibration foil could be measured against $I_1$. A potential of 1600 V was applied in series to the ionization chambers. Samples were calibrated in situ to the energy of the first inflection point of the K-edge of an yttrium foil (17,038.4 eV).

The X-ray absorption near edge spectra (XANES) were measured at the SSRL, under dedicated operating conditions (3.0 GeV, 5%, 500 mA using continuous top-off injections) on end station 11-2. This beamline was equipped with a 26-pole, 2.0 T wiggler, utilized a liquid nitrogen-cooled double-crystal Si(220) monochromator, and employed collimating and focusing mirrors. A single energy was selected from the white beam with a liquid-$N_2$-cooled double-crystal monochromator utilizing Si(220) ($\varphi$ = 0) crystals. Although the crystals were run fully tuned, higher harmonics from the monochromatic light were removed using a 370 mm Rh-coated harmonic rejection mirror. The Rh coating was 50 nm with 20 nm seed coating, and the substrate was Zerodur. Vertical acceptance was controlled by slits positioned before the monochromator. The harmonic rejection cutoff was set by the mirror angle, thereby controlling which photons experience total external reflection. The horizontal and vertical slit sizes were 15 and 1 mm, respectively (10 mm horizontal slit for $Cs_2UO_2Cl_4$). The XAS spectra were collected as a true absorption measurement, $\ln(I_0/I_1)$.

Data were treated as previously described.[17,22,34] Data were background subtracted by fitting a line to the pre-edge region, which was subsequently subtracted from the experimental data to eliminate the background. Data were normalized by fitting a first-order polynomial to the postedge region of the spectrum and setting the edge jump to an intensity of 1.0.

**Preparation of $H_2$($^{Mes}$DAE).** A 500 mL round-bottom flask was charged with *N,N′*-dimesitylethane-1,2-diamine dihydrochloride (1.750 g, 4.74 mmol) and 300 mL of a saturated, aqueous $NaHCO_3$ solution. This suspension was stirred until approximately 90% of the solid was dissolved (1 h) before the product was extracted with dichloromethane (3 × 200 mL). After the dichloromethane solution was dried over $MgSO_4$ and concentrated in vacuo, a clear, colorless oil was obtained, which solidified overnight to a crystalline, white solid assigned as $H_2$($^{Mes}$DAE) (1.100 g, 3.71 mmol, 78%). $^1$H NMR spectrum in $CD_3Cl$ matches previously published data.[45] $^1$H NMR ($C_6D_6$, 25 °C): $\delta$ = 2.18 (s, 6H, $CH_3$), 2.22 (s, 12H, $CH_3$), 2.95 (s, 4H, $CH_2$), 3.40 (bs, 2H, N*H*), 6.79 (s, 4H, Ar–C*H*).

**Preparation of ($^{Mes}$DAE)$_2$U(THF) (1-DAE).** A 20 mL scintillation vial was charged with $H_2$($^{Mes}$DAE) (0.468 g, 1.58 mmol) and 15 mL of THF. An orange solution of $KCH_2Ph$ (0.414 g, 3.18 mmol) in 5 mL of THF was added dropwise to the $H_2$($^{Mes}$DAE) solution, causing a color change from colorless to yellow. After being stirred for 10 min, a yellow solid suddenly precipitated from the solution. This suspension was then added dropwise to a 100 mL round-bottom flask containing a green solution of $UCl_4$ (0.300 g, 0.790 mmol) in 30 mL of THF, causing an immediate color change to dark orange. After being stirred for 1 h, the solution was concentrated in vacuo to a sticky, orange solid. Pentane (80 mL) was added, and the solution was allowed to stir for 1 h before KCl was removed by filtration. The resulting yellow solution was concentrated to 10 mL and cooled to −35 °C, causing the precipitation of a yellow solid. After the pentane was decanted, the yellow solid was dried in vacuo and assigned as ($^{Mes}$DAE)$_2$U(THF) (**1-DAE**) (0.330 g, 0.367 mmol, 46%). Brown crystals suitable for X-ray analysis were grown by slow evaporation from diethyl ether at −35 °C. Analysis for $C_{44}H_{60}N_4OU$: Calcd C, 58.78; H, 6.73; N, 6.23. Found C, 58.61; H, 6.79; N, 6.42. $^1$H NMR ($C_6D_6$, 25 °C): $\delta$ = −15.88 (38, 24H, $CH_3$), 5.61 (12, 12H, $CH_3$), 10.71 (15, 8H, Ar–C*H*), 62.03 (31, 8H, $CH_2$).

**Preparation of Cp$_2$U($^{Mes}$DAE) (2-DAE).** A 20 mL scintillation vial was charged with $H_2$($^{Mes}$DAE) (0.234 g, 0.789 mmol) and 10 mL of THF. An orange solution of $KCH_2Ph$ (0.207 g, 1.59 mmol) in 5 mL of THF was added dropwise to the $H_2$($^{Mes}$DAE) solution, causing a color change from colorless to yellow. After being stirred for 10 min, a yellow solid suddenly precipitated from the solution. This suspension was then added dropwise to a 100 mL round-bottom flask containing a green solution of $UCl_4$ (0.300 g, 0.790 mmol) in 30 mL of THF, causing an immediate color change to dark orange. Quickly, NaCp (0.138 g, 1.57 mmol) was added as a solid, causing the solution to darken. After being stirred for 1 h, the solution was concentrated in vacuo to a sticky, brown solid. A total of 80 mL of pentane was added, and the solution was allowed to stir for 1 h before KCl and NaCl were removed by filtration. The resulting orange solution was concentrated to 10 mL and cooled to −35 °C causing the precipitation of an orange solid. After the pentane was decanted, the orange solid was dried in vacuo and assigned as Cp$_2$U($^{Mes}$DAE) (**2-DAE**) (0.212 g, 0.307 mmol, 39%). Orange crystals suitable for X-ray analysis were grown from a concentrated pentane solution at −35 °C overnight. Analysis for $C_{30}H_{36}N_4U$: Calcd C, 54.38; H, 5.48; N, 4.23. Found C, 54.27; H, 5.65; N, 4.47. $^1$H NMR ($C_6D_6$, 25 °C): $\delta$ = −11.53 (6, 12H, $CH_3$), 1.18 (13, 6H, $CH_3$), 1.35 (9, 10H, Cp–C*H*), 4.32 (4, 4H, Ar–C*H*), 31.12 (8, 4H, $CH_2$).

## ■ RESULTS AND DISCUSSION

**Synthesis of Redox-Innocent Analogues.** Herein, we prepared molecular systems where redox-active and redox-innocent ligands can be directly compared on uranium. To achieve this, we designed a ligand that would retain the steric properties of $^{Mes}$DAB$^{Me}$ while providing amide linkages to uranium via amine deprotonation. We proposed the most straightforward method for the amine synthesis would be by reduction of $^{Mes}$DAB$^{Me}$ with sodium borohydride. However, upon workup, the complexity associated with separation of diastereomers precluded a suitable platform for scalable chemistry. Thus, we selected a ligand with an ethylenediamine backbone, which eliminates diastereomer formation, but still allows installation of the bulky mesityl groups. This ligand was prepared by deprotonating the previously synthesized *N,N′*-dimesitylethane-1,2-diamine dihydrochloride with excess sodium bicarbonate, which generates $H_2$($^{Mes}$DAE) in moderate yield as a colorless oil.[41] In its purest form, $H_2$($^{Mes}$DAE) solidifies over the course of days, but no difference in spectroscopic properties or metalation reactivity was observed between the two phases of matter.

Deprotonation of 2 equiv of $H_2$($^{Mes}$DAE) was accomplished in situ using 4 equiv of benzyl potassium in THF (eq 1), signified by precipitation of a yellow solid. Addition of this

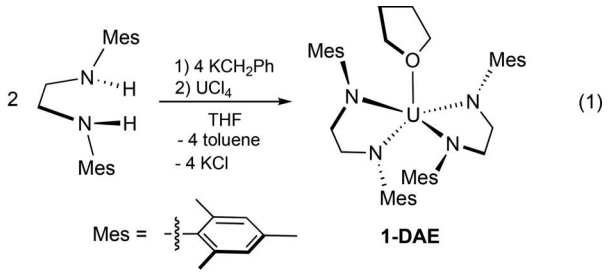

(1)

suspension to 1 equiv of $UCl_4$ in THF at room temperature generated a dark-orange solution. Following concentration of the solution, extraction, and recrystallization from pentane, ($^{Mes}$DAE)$_2$U(THF) (**1-DAE**) was isolated as a yellow powder in moderate yield. It should be noted that using this ligand solution for metalation prior to ligand precipitation left substantial H$_2$($^{Mes}$DAE) impurities in the final product. Analysis of a KBr pellet of **1-DAE** by IR spectroscopy confirmed that no N−H functionalities were present (Figure S4).

Analysis of **1-DAE** by $^1$H NMR spectroscopy reveals a sharp, paramagnetically shifted, $C_{2v}$-symmetric spectrum. All mesityl groups appeared equivalent. Resonances at −15.88 and 5.61 ppm correspond to the methyl groups of the mesityl substituents, while a resonance at 10.71 ppm is observed for the aryl protons of the mesityl groups. An additional downfield shifted resonance is observed at 62.03 ppm corresponding to the backbone methylene groups. Similar to **1-DAB**, no THF resonances are observed in the spectrum at room temperature; however, addition of excess pyridine-$d_5$ to a known amount of **1-DAE** liberated 1 equiv of THF, as determined by $^1$H NMR spectroscopy by integration with a mesitylene standard. The THF resonances are likely not observable at room temperature due to broadening from dynamic behavior.

The sharpness and symmetry observed in the $^1$H NMR spectrum of **1-DAE** contrast that of **1-DAB**, which has very broad resonances. The origin of this broadness was proposed to originate from dynamic behavior in benzene-$d_6$ solution at ambient temperature. It seems likely that the uranium is interacting with one of the ligand "ene" backbones in solution. This interpretation was supported by sharpening of the resonances in the low temperature $^1$H NMR spectrum (toluene-$d_8$, 10 °C).[34]

Following the isolation of **1-DAE**, the redox-innocent ligand analogue to **2-DAB**, Cp$_2$U($^{Mes}$DAE) (**2-DAE**), was targeted. Synthesis was again accomplished by in situ deprotonation of 1 equiv of H$_2$($^{Mes}$DAE) in THF, followed by transfer of this slurry to a THF solution of $UCl_4$ with subsequent quick addition of 2 equiv of solid NaCp (eq 2). Following workup, **2-DAE** was

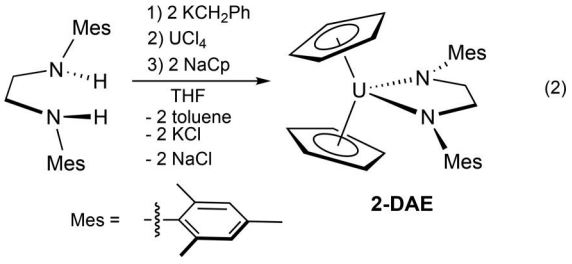

(2)

isolated in moderate yield as an orange powder. The new compound was characterized by IR spectroscopy to confirm the absence of N−H functional groups (Figure S5).

The $^1$H NMR spectrum of **2-DAE** was reminiscent of **1-DAE**, again showing sharp, paramagnetically shifted resonances and an overall $C_{2v}$-symmetric spectrum. Resonances assigned to the methyl groups for the mesityl substituents are observed at −11.53 and 1.18 ppm, while the aryl protons on the mesityl rings appear at 4.32 ppm. A large resonance, observed at 1.35 ppm, is assignable to the Cp protons, whereas the backbone methylene protons appear downfield (31.12 ppm). The symmetry of **2-DAE** in solution contrasts that of the analogous $^{Mes}$DAB$^{Me}$ compound, as **2-DAB** displays a $C_s$-symmetric spectrum, likely resulting from a static backbone interaction in solution that is missing in **2-DAE**.

**X-ray Crystallography.** The molecular structures of newly generated **1-DAE** and **2-DAE** compounds were interrogated by single crystal X-ray diffraction measurements. The results were directly compared with the **1-DAB** and **2-DAB** analogues. Although the symmetries of the $^{Mes}$DAE and $^{Mes}$DAB$^{Me}$ series differ in solution, for this study it is imperative that the solid-state geometries are analogous to eliminate ligand electronic influences other than the ligand backbone interactions. Furthermore, since a majority of the electronic characterization techniques are performed on solid-state samples, X-ray crystallographic analysis will aid in understanding structural elements and possible molecular interactions.

Brown crystals of compound **1-DAE** suitable for single crystal X-ray diffraction analysis were grown by slow evaporation from a concentrated diethyl ether solution at −35 °C. Refinement of the data confirmed the identity of **1-DAE** as ($^{Mes}$DAE)$_2$U(THF) (Figure 2, right; Table 1). Slight structural deviations are noted between **1-DAB** and **1-DAE**. While **1-DAB** is consistent with a distorted trigonal bipyramidal geometry ($\tau$ = 0.735), **1-DAE** is more consistent with a distorted square pyramidal geometry ($\tau$ = 0.305).

The U−N bond distances of **1-DAE**, ranging from 2.242(2)−2.264(2) Å, are consistent with those observed in **1-DAB** (2.251(4)−2.255(4) Å) and indicative of anionic uranium−nitrogen interactions. From the structural parameters, it is also evident that the C−C bonds in the backbone of the $^{Mes}$DAE ligands are consistent with C−C single bonds, displaying distances of 1.523(4) and 1.529(4) Å. These values differ significantly from those of the C=C bonds (1.361(8) and 1.364(7) Å) in **1-DAB**.[46−49] Additionally, in compound **1-DAE** the U−C contacts are too long (ranging from 3.022(3) to 3.171 Å) to be considered as bonded; this contrasts the U−C distances of **1-DAB**, which are much shorter at 2.749(5) to 2.788(5) Å and are clearly interacting.[50]

Single orange crystals of compound **2-DAE** suitable for X-ray crystallography were grown from a concentrated pentane solution at −35 °C overnight. Analysis confirmed the identity of **2-DAE** as Cp$_2$U($^{Mes}$DAE) (Figure 3, right; Table 1), featuring a distorted tetrahedral geometry (when considering the Cp centroids) similar to **2-DAB**.

The U−N distances in **2-DAE** (2.221(3) and 2.204(3) Å) are consistent with those observed in **2-DAB** (2.224(6) and 2.198(6) Å) and are indicative of anionic uranium−nitrogen interactions. Charge balancing suggests that **2-DAE** contains a U(IV) cations. Similar to compound **1-DAE**, the C−C bond distance in the ligand backbone of compound **2-DAE** (1.540(5) Å) is consistent with a C−C single bond, again contrasting the C=C double bond in the backbone of **2-DAB** (1.399(11) Å). As for **1-DAE**, the uranium interaction with the ligand backbone is diminished in compound **2-DAE**, as the U−C

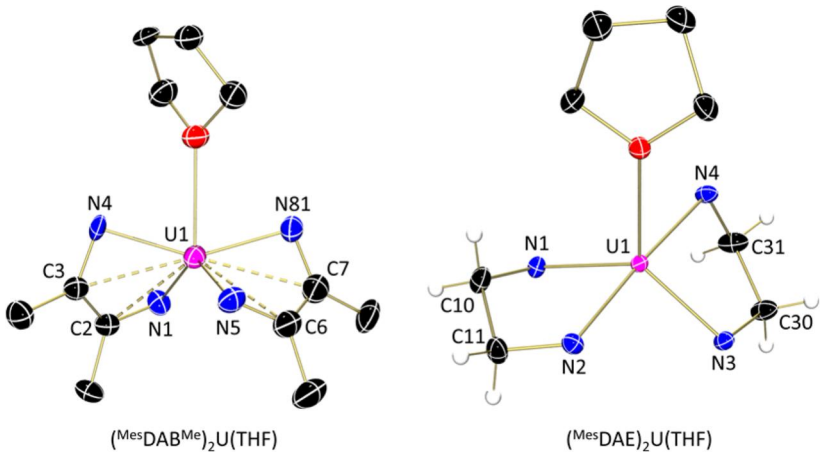


**Figure 2.** Molecular structures of ($^{Mes}$DAB$^{Me}$)$_2$U(THF) (**1-DAB**)[34] and ($^{Mes}$DAE)$_2$U(THF) (**1-DAE**) shown with 30% probability ellipsoids. Selected hydrogen atoms, solvent molecules, and mesityl groups have been omitted for clarity.

**Table 1. Bond Distances (in Å) for $^{Mes}$DAB$^{Me}$ and $^{Mes}$DAE Compounds**[34]

| compound | C−N | C−C | U−N | U−C$_{backbone}$ |
|---|---|---|---|---|
| ($^{Mes}$DAB$^{Me}$)$_2$U(THF) (**1-DAB**) | 1.431(7) | 1.361(8) | 2.251(4) | 2.749(5) |
| | 1.419(6) | 1.364(7) | 2.252(4) | 2.773(4) |
| | 1.432(6) | | 2.255(3) | 2.787(6) |
| | 1.418(6) | | 2.255(4) | 2.788(5) |
| ($^{Mes}$DAE)$_2$U(THF) (**1-DAE**) | 1.485(4) | 1.523(4) | 2.264(2) | 3.022(3) |
| | 1.471(4) | 1.529(4) | 2.242(2) | 3.141(3) |
| | 1.477(4) | | 2.264(2) | 3.171(3) |
| | 1.466(4) | | 2.259(2) | 3.058(3) |
| Cp$_2$U($^{Mes}$DAB$^{Me}$) (**2-DAB**) | 1.425(10) | 1.399(11) | 2.224(6) | 2.637(7) |
| | 1.407(9) | | 2.198(6) | 2.685(5) |
| Cp$_2$U($^{Mes}$DAE) (**2-DAE**) | 1.473(4) | 1.540(5) | 2.221(3) | 3.069(3) |
| | 1.495(4) | | 2.204(3) | 2.874(3) |

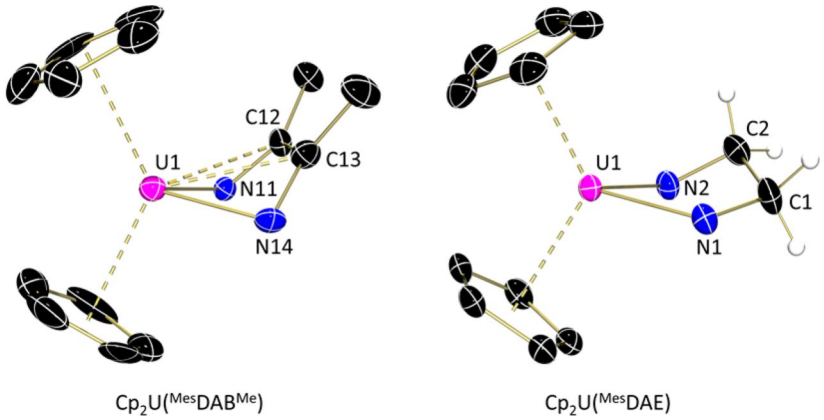


**Figure 3.** Molecular structures of Cp$_2$U($^{Mes}$DAB$^{Me}$) (**2-DAB**)[34] and Cp$_2$U($^{Mes}$DAE) (**2-DAE**) shown with 30% probability ellipsoids. Select hydrogen atoms, solvent molecules, and mesityl groups have been omitted for clarity.

distances of 2.875 and 3.068 Å are substantially longer than those noted in **2-DAB** (2.637(7) to 2.685(5) Å).

**Electronic Absorption Spectroscopy.** To corroborate our oxidation state assignment of U(IV) for both **1-DAE** and **2-DAE**, as well as to serve as a comparison to the $^{Mes}$DAB$^{Me}$ derivatives, electronic absorption spectroscopy was performed. Spectra for **1-DAE** and **2-DAE** were recorded in THF solution at room temperature in both the UV−visible (Figure 4, left) and near-infrared regions (Figure 4, right). In the UV−visible region, both **1-DAE** and **2-DAE** have nearly featureless spectra, except for absorbances around 300 nm that are only partially discernible. These absorbances are likely charge-transfer bands and are consistent with those observed for the $^{Mes}$DAB$^{Me}$ compounds.[34] Similarly, the near-IR region shows sharp but weakly intense bands that are characteristic of f−f transitions typically observed for U(IV), f$^2$ complexes.[51,52]

**X-ray Absorption Spectroscopy.** The effective nuclear charge on uranium within a series of compounds containing redox-active $^{Mes}$DAB$^{Me}$ versus redox-innocent $^{Mes}$DAE ligands was compared using X-ray absorption near edge structure (XANES) spectroscopy (Figure 5). The U L$_3$-edge XANES spectra for **1-DAE**, **1-DAB**, **2-DAE**, and **2-DAB** collected at 80

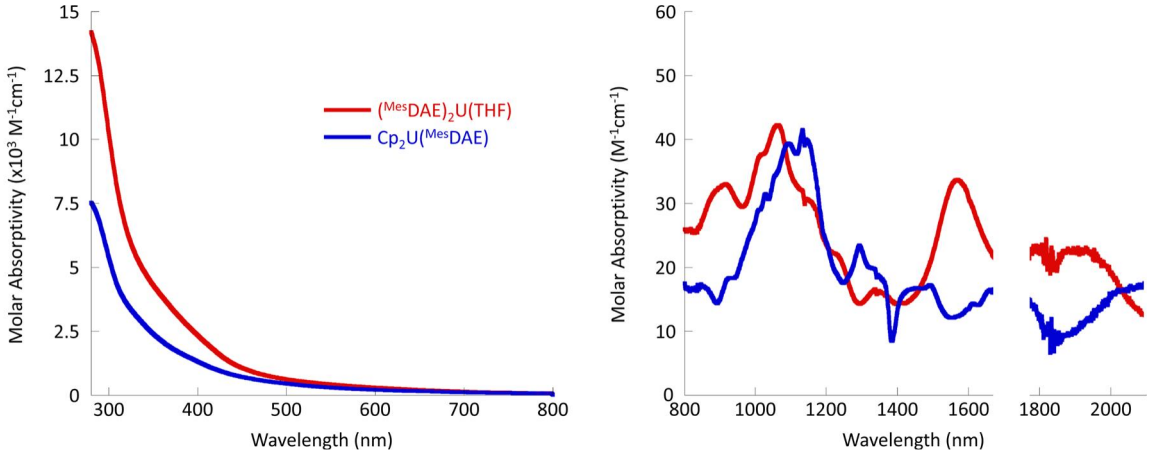


**Figure 4.** Electronic absorption spectra in the UV−visible region (left) and near-infrared region (right) for $(^{Mes}DAE)_2U(THF)$ (**1-DAE**) and $Cp_2U(^{Mes}DAE)$ (**2-DAE**) in THF at ambient temperature. THF solvent overtones between 1675 and 1775 nm have been omitted for clarity.

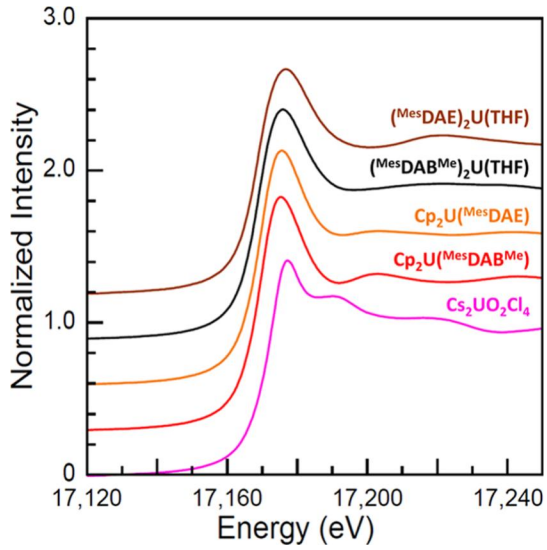


**Figure 5.** U $L_3$-edge XANES spectra from $Cs_2UO_2Cl_4$ (pink), **1-DAE** (brown), **1-DAB** (black), **2-DAE** (orange), and **2-DAB** (red) collected at 80 K.

K were background subtracted and normalized. As characteristic for U $L_3$-edge XANES,[17,53−56] each spectrum was dominated by a large edge feature superimposed on a step-like absorption threshold. It has been shown that the energy of this absorption peak can be correlated with the effective nuclear charge of the absorbing uranium atom.[34,55,57−60] Data were calibrated in energy to the inflection point of the Y K-edge XANES spectrum from an Y foil measured in situ (17038.4 eV). Note, the **1-DAB** and **2-DAB** compounds were measured in 2011, but the original spectra were referenced to 17032.08 eV, not the more conventional 17038.4 eV. For this reason, the $^{Mes}DAB^{Me}$ compounds were re-evaluated experimentally in this study, and the results are presented herein. To ensure robust calibration, the U $L_3$-edge XANES energies were additionally evaluated against an external standard, namely, $Cs_2UO_2Cl_4$. Not only does this external calibration standard guard against energy drift over time (accompanying oxidation of the Y calibration foil), it also facilitates comparison of inflection point measurements previously reported in the literature.[53,57]

Edge-positions for the four analytes were characterized by their individual inflection points (Table 2). These values were defined by the point at which the second derivative of the data equaled zero. Overall, the analytes' inflection points were similar in energy, spanning only 1 eV. Uncertainty associated with such inflection point measurements is typically between ±0.5 and 0.1 eV. All inflection point values were on the order of 4.2 to 2.8 eV lower in energy than the $Cs_2UO_2Cl_4$ external standard, consistent with the uranium ions being described as +4.[53] For **1-DAB** and **2-DAB**, the measured 17169.3 ± 0.1 and 17169.7 ± 0.6 eV inflections points were equivalent to that observed in 2011 (i.e., 17169.3 eV), once the experimental uncertainties were considered. The inflection point energies showed no statistically relevant dependence on diamide identity, comparing reduced $^{Mes}DAB^{Me}$ to $^{Mes}DAE$. However, the inflection point energies dropped by 0.4 to 0.7 eV when changing from a combination of a single diamide with two cyclopentadienides (**2-DAE**) to a ligand environment comprised of two diamides and a THF molecule (**1-DAE**). The peak maxima (where the first derivative of the data equaled zero) were also determined. Again, these values spanned a small energy range (only 0.9 eV). Like the inflection points, the peak

**Table 2. U $L_3$-Edge XANES Data from 1-DAE, 1-DAB, 2-DAE, and 2-DAB**

| compound | inflection point[a] | analyte inflection point minus that of $Cs_2UO_2Cl_4$ | peak maxima |
|---|---|---|---|
| $Cs_2UO_2Cl_4$ | 17173.2 ± 0.2 | 0 | 17177.3 ± 0.2 |
| $Cp_2U(^{Mes}DAE)$ (**2-DAE**) | 17170.4 ± 0.6 | −2.8 | 17175.8 ± 0.2 |
| $Cp_2U(^{Mes}DAB^{Me})$ (**2-DAB**) | 17169.7 ± 0.5 | −3.5 | 17175.4 ± 0.2 |
| $(^{Mes}DAB^{Me})_2U(THF)$ (**1-DAB**) | 17169.3 ± 0.1 | −3.9 | 17176.8 ± 0.2 |
| $(^{Mes}DAE)_2U(THF)$ (**1-DAE**) | 17169.0 ± 0.1 | −4.2 | 17176.7 ± 0.2 |

[a]Inflection points and peak maxima are included (eV), as well as the inflection point energy differences between the analyte and the $Cs_2UO_2Cl_4$ external standard. All data were calibrated against the Y K-edge from an Y foil measured in situ (17038.4 eV).

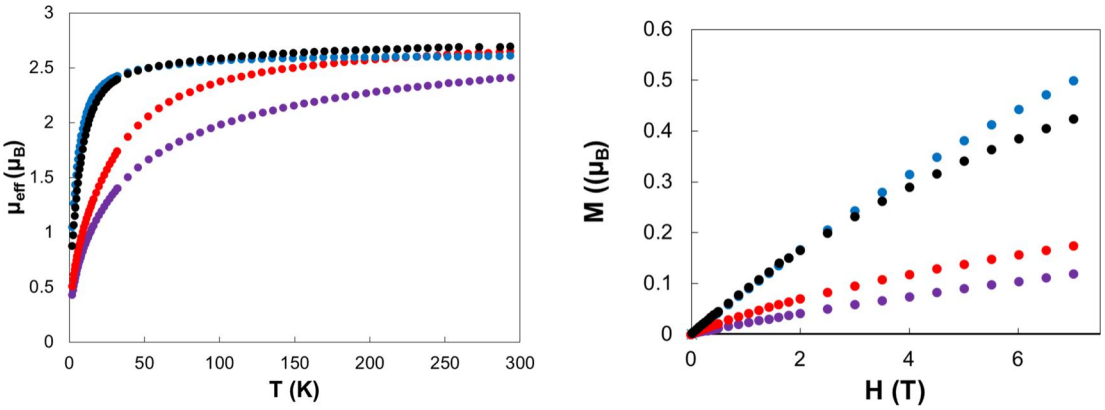


**Figure 6.** Temperature (left) and field-dependent (right) magnetic data for ($^{Mes}$DAE)$_2$U(THF) (**1-DAE**) (black), ($^{Mes}$DAB$^{Me}$)$_2$U(THF) (**1-DAB**) (blue), Cp$_2$U($^{Mes}$DAE) (**2-DAE**) (red), and Cp$_2$U($^{Mes}$DAB$^{Me}$) (**2-DAB**) (purple). Temperature-dependent data were collected at 1.0 T, and field-dependent data at 2 K.

maxima could be grouped in pairs, compounds **1** vs compounds **2**. However, in contrast to the inflection point measurements, moving from compounds **2** to compounds **1** causes an approximate increase (not a decrease) in peak maxima energy of 1.2 eV, which was statistically relevant. This energy shift highlights electronic structure differences between metallocene and bis(diamide) ligand environments. Unfortunately, the resolutions associated with the U $L_3$-edge measurement were not sufficiently rigorous to evaluate the exact origin of this energy shift. Hence, we conclude from X-ray absorption spectroscopy that the switch to redox-innocent ligands imparted negligible electronic differences on the uranium cations in these complexes. In other words, the redox-active ligands in this system do not appear to significantly contribute to covalency at the uranium, in contrast to transition metal examples.[13,15,31,32,61,62]

**Magnetism.** To further compare the electronic structures of compounds **1-DAE** and **2-DAE** to the previously reported unsaturated analogues, **1-DAB** and **2-DAB**, magnetic data were collected. Temperature-dependent data for compounds **1-DAE** and **2-DAE** were collected at 1 T in the range of 2−300 K (Figure 6, left). The data were consistent with a simple $5f^2$ U(IV) cation as evidenced by the low temperature moments of 0.51 and 0.88 $\mu_B$, which increased to 2.64 and 2.69 $\mu_B$ at room temperature. These low and room temperature moments, as well as the overall line-shape, are consistent with data reported for many other U(IV) complexes.[63] Additionally, field-dependent data at 2 K were collected from 0−7 T (Figure 6, right), which revealed low moments consistent with singlet ground states, expected for uranium(IV) complexes.[64−66]

Previously, the temperature- and field-dependent data for **1-DAB** and **2-DAB** were reported with samples prepared using annealed gelatin capsules as sample holders.[34] While it has been shown that simple room temperature moments are not diagnostic tools alone for assigning oxidation states of uranium cations,[63] the room temperature moments for **1-DAB** and **2-DAB** were surprisingly low for U(IV) cations at 1.91 and 1.79 $\mu_B$, respectively. The low moments were purported to arise as a result of an electronic effect from the direct structural interaction between the ene-diamide ligands and uranium cations.[34]

For the current work, magnetism data for **1-DAB** and **2-DAB** were recollected using very low background plastic straw sample holders described in the Experimental Section, for consistency with the sample preparation that was used in the data collection for **1-DAE** and **2-DAE** (Figure 6). These measurements revealed little difference between **1-DAE** and **1-DAB**, and between **2-DAE** and **2-DAB** respectively. These new results are at odds with the previous report. Upon examining the new data, **1-DAB** has a low temperature moment of 1.04 $\mu_B$ that increases to 2.61 $\mu_B$ at room temperature. These values are quite consistent with **1-DAE**, which has a low temperature moment of 0.88 $\mu_B$ and achieves a moment of 2.69 $\mu_B$ at room temperature. Additionally, upon comparing the temperature dependent data for **2-DAB** and **2-DAE**, similar moments of 0.43 and 0.51 $\mu_B$ at 2 K, and moments of 2.41 and 2.64 at room temperature are observed. Field-dependent plots attained low moments for all of the derivatives without saturation. In light of these new measurements, it can be concluded that **1-DAB** and **2-DAB**, which have the potential to have redox-active ligand systems, have electronic structures that are very similar to those of **1-DAE** and **2-DAE**, which contain redox-innocent ligand frameworks. Furthermore, the low moments we reported previously emerged from experimental artifacts associated with the sample holders.

## ■ CONCLUSION

Compounds **1-DAE** and **2-DAE**, which possess redox-innocent ligands, were synthesized as analogues to ($^{Mes}$DAB$^{Me}$)$_2$U(THF) (**1-DAB**) and Cp$_2$U($^{Mes}$DAB$^{Me}$) (**2-DAB**), which contain redox-active, $\alpha$-diimine ligands that were fully reduced to their ene-diamide forms. Crystallographic analysis determined that the uranium ions in both **1-DAE** and **2-DAE** were structurally analogous to their redox-active counterparts, differing only by the absence of ligand backbone interactions in the redox-innocent series. This allowed for a detailed analysis of the electronic effects imparted by the interaction of the $\pi$-system with the uranium center.

Analysis of **1-DAE** and **2-DAE** using the same spectroscopic techniques as **1-DAB** and **2-DAB** allowed for a direct comparison to elucidate the bonding and electronic structure between the two families of compounds. Data obtained from electronic absorption spectroscopy, X-ray absorption spectroscopy, and magnetic measurements are all in agreement, suggesting that the additional $^{Mes}$DAB$^{Me}$ ligand interaction in the ene-diamide form has a negligible electronic influence on the uranium center. Furthermore, the updated magnetic data now show magnetic moments consistent with typical uranium-(IV) species. Thus, there is no covalency imparted to uranium

from using the redox-active $\alpha$-diimine ligand, $^{Mes}DAB^{Me}$. This is in contrast to transition metals, where large degrees of electron delocalization are noted when redox active ligands are utilized. Currently, we are studying other redox-active ligand systems in a similar fashion to better understand the electronic demands of these ligands, allowing us to more effectively understand bonding in actinide complexes with organic ligands.

### Accession Codes

CCDC 1822206–1822207 (**1-DAE** and **2-DAE**) contain the supplementary crystallographic data for this paper. These data can be obtained free of charge via www.ccdc.cam.ac.uk/data_request/cif, or by emailing data_request@ccdc.cam.ac.uk, or by contacting The Cambridge Crystallographic Data Centre, 12 Union Road, Cambridge CB2 1EZ, UK; fax: +44 1223 336033.

## ■ AUTHOR INFORMATION


### Corresponding Author

*E-mail: sbart@purdue.edu.

### ORCID ●

Eric J. Schelter: 0000-0002-8143-6206
Maryline G. Ferrier: 0000-0003-0081-279X
Sharon E. Bone: 0000-0002-7521-9627
Suzanne C. Bart: 0000-0002-8918-9051


### Notes

The authors declare no competing financial interest.

## ■ ACKNOWLEDGMENTS


This material is based upon work supported by the U.S. Department of Energy, Office of Science, Division of Chemical Sciences, Geosciences, and Biosciences, Office of Basic Energy Sciences, Heavy Element Chemistry Program by grants to S.C.B. (DE-SC0008479) and S.A.K./J.S.L.P. as well as the Separation Science Program by a grant to E.J.S. (DE-SC0017259). Portions of this work were supported by postdoctoral fellowships from the Glenn T. Seaborg Institute (M.G.F., B.W.S.) and the Agnew National Security Fellowship (S.E.B.). Los Alamos National Laboratory is operated by Los Alamos National Security, LLC, for the National Nuclear Security Administration of U.S. Department of Energy (Contract DE-AC52-06NA25396). Use of the Stanford Synchrotron Radiation Lightsource, SLAC National Accelerator Laboratory, was supported by the U.S. Department of Energy, Office of Science, Office of Basic Energy Sciences under Contract No. DE-AC02-76SF00515. The X-ray crystallographic data in this work was obtained on instruments funded by the National Science Foundation (Grant CHE-0087210), Ohio Board of Regents (Grant CAP-491) and by Youngstown State University. Dr. Steven Kraft and Dr. Xikang Zhao are acknowledged for preliminary experiments related to this work.


## ■ REFERENCES


(1) Chirik, P. J. Iron- and Cobalt-Catalyzed Alkene Hydrogenation: Catalysis with Both Redox-Active and Strong Field Ligands. *Acc. Chem. Res.* **2015**, *48*, 1687–1695.

(2) Luca, O. R.; Crabtree, R. H. Redox-Active Ligands in Catalysis. *Chem. Soc. Rev.* **2013**, *42*, 1440–1459.

(3) Kaim, W. The Shrinking World of Innocent Ligands: Conventional and Non-Conventional Redox-Active Ligands. *Eur. J. Inorg. Chem.* **2012**, *2012*, 343–348.

(4) Eisenberg, R.; Gray, H. B. Non-innocence in Metal Complexes: A Dithiolene Dawn. *Inorg. Chem.* **2011**, *50*, 9741–9751.

(5) Chirik, P. J. Preface: Forum on Redox-Active Ligands. *Inorg. Chem.* **2011**, *50*, 9737–9740.

(6) Chirik, P. J.; Wieghardt, K. Radical Ligands Confer Nobility on Base-Metal Catalysts. *Science* **2010**, *327*, 794–795.

(7) Broere, D. L. J.; Plessius, R.; van der Vlugt, J. I. New Avenues for Ligand-Mediated Processes - Expanding Metal Reactivity by the Use of Redox-Active Catechol, *o*-Aminophenol and *o*-Phenylenediamine Ligands. *Chem. Soc. Rev.* **2015**, *44*, 6886–6915.

(8) Praneeth, V. K. K.; Ringenberg, M. R.; Ward, T. R. Redox-Active Ligands in Catalysis. *Angew. Chem., Int. Ed.* **2012**, *51*, 10228–10234.

(9) Sarkar, B.; Schweinfurth, D.; Deibel, N.; Weisser, F. Functional Metal Complexes Based on Bridging "Imino"-Quinonoid Ligands. *Coord. Chem. Rev.* **2015**, *293–294*, 250–262.

(10) Bejger, C.; Tian, Y.-H.; Barker, B. J.; Boland, K. S.; Scott, B. L.; Batista, E. R.; Kozimor, S. A.; Sessler, J. L. Synthesis and Characterization of a Tetrathiafulvalene-Salphen Actinide Complex. *Dalton Trans.* **2013**, *42*, 6716–6719.

(11) Tezgerevska, T.; Alley, K. G.; Boskovic, C. Valence Tautomerism in Metal Complexes: Stimulated and Reversible Intramolecular Electron Transfer between Metal Centers and Organic Ligands. *Coord. Chem. Rev.* **2014**, *268*, 23–40.

(12) Warren, L. F. Synthesis of [M'-N4] and [M'-N6] Complexes Based on *o*-Benzoquinone Diimine with Cobalt, Iron, and Ruthenium. *Inorg. Chem.* **1977**, *16*, 2814–2819.

(13) De Bruin, B.; Bill, E.; Bothe, E.; Weyhermüller, T.; Wieghardt, K. Molecular and Electronic Structures of Bis(Pyridine-2,6-Diimine)-Metal Complexes $[ML_2](PF_6)_n$ ($n$ = 0, 1, 2, 3; M = Mn, Fe, Co, Ni, Cu, Zn). *Inorg. Chem.* **2000**, *39*, 2936–2947.

(14) Bill, E.; Beckmann, U.; Wieghardt, K. Electronic and Molecular Structure Studies of a (Bio)Inorganic Complex - A Multi-Technique Approach. *Hyperfine Interact.* **2003**, *144–145*, 183–198.

(15) Ranis, L. G.; Werellapatha, K.; Pietrini, N. J.; Bunker, B. A.; Brown, S. N. Metal and Ligand Effects on Bonding in Group 6 Complexes of Redox-Active Amidodiphenoxides. *Inorg. Chem.* **2014**, *53*, 10203–10216.

(16) Olivos Suarez, A. I.; Lyaskovskyy, V.; Reek, J. N. H.; van der Vlugt, J. I.; de Bruin, B. B. Complexes with Nitrogen-Centered Radical Ligands: Classification, Spectroscopic Features, Reactivity, and Catalytic Applications. *Angew. Chem., Int. Ed.* **2013**, *52*, 12510–12529.

(17) Kiernicki, J. J.; Ferrier, M. G.; Lezama Pacheco, J. S. L.; La Pierre, H. S. L.; Stein, B. W.; Zeller, M.; Kozimor, S. A.; Bart, S. C. Examining the Effects of Ligand Variation on the Electronic Structure of Uranium Bis(Imido) Species. *J. Am. Chem. Soc.* **2016**, *138*, 13941–13951.

(18) Kiernicki, J. J.; Cladis, D. P.; Fanwick, P. E.; Zeller, M.; Bart, S. C. Synthesis, Characterization, and Stoichiometric U = O Bond Scission in Uranyl Species Supported by Pyridine(Diimine) Ligand Radicals. *J. Am. Chem. Soc.* **2015**, *137*, 11115–11125.

(19) Kiernicki, J. J.; Newell, B. S.; Matson, E. M.; Anderson, N. H.; Fanwick, P. E.; Shores, M. P.; Bart, S. C. Multielectron C-O Bond Activation Mediated by a Family of Reduced Uranium Complexes. *Inorg. Chem.* **2014**, *53*, 3730–3741.

(20) Kiernicki, J. J.; Fanwick, P. E.; Bart, S. C. Utility of a Redox-Active Pyridine(Diimine) Chelate in Facilitating Two Electron Oxidative Addition Chemistry at Uranium. *Chem. Commun.* **2014**, *50*, 8189–8192.

(21) Pattenaude, S. A.; Kuehner, C. S.; Dorfner, W. L.; Schelter, E. J.; Fanwick, P. E.; Bart, S. C. Spectroscopic and Structural Elucidation of

Uranium Dioxophenoxazine Complexes. *Inorg. Chem.* **2015**, *54*, 6520−6527.
(22) Anderson, N. H.; Odoh, S. O.; Williams, U. J.; Lewis, A. J.; Wagner, G. L.; Lezama Pacheco, J.; Kozimor, S. A.; Gagliardi, L.; Schelter, E. J.; Bart, S. C. Investigation of the Electronic Ground States for a Reduced Pyridine(Diimine) Uranium Series: Evidence for a Ligand Tetraanion Stabilized by a Uranium Dimer. *J. Am. Chem. Soc.* **2015**, *137*, 4690−4700.
(23) Camp, C.; Mougel, V.; Horeglad, P.; Pecaut, J.; Mazzanti, M. Multielectron Redox Reactions Involving C-C Coupling and Cleavage in Uranium Schiff Base Complexes. *J. Am. Chem. Soc.* **2010**, *132*, 17374−17377.
(24) Fedushkin, I. L.; Maslova, O. V.; Lukoyanov, A. N.; Fukin, G. K. Anionic and Neutral Bis(Diimine)Lanthanide Complexes. *C. R. Chim.* **2010**, *13*, 584−592.
(25) Mullane, K. C.; Cheisson, T.; Nakamaru-Ogiso, E.; Manor, B. C.; Carroll, P. J.; Schelter, E. J. Reduction of Carbonyl Groups by Uranium(III) and Formation of a Stable Amide Radical Anion. *Chem. - Eur. J.* **2018**, *24*, 826−837.
(26) Fang, H.; Cole, B. E.; Qiao, Y.; Bogart, J. A.; Cheisson, T.; Manor, B. C.; Carroll, P. J.; Schelter, E. J. Electro-Kinetic Separation of Rare Earth Elements Using a Redox-Active Ligand. *Angew. Chem., Int. Ed.* **2017**, *56*, 13450−13454.
(27) Anderson, N. H.; Odoh, S. O.; Yao, Y.; Williams, U. J.; Schaefer, B. A.; Kiernicki, J. J.; Lewis, A. J.; Goshert, M. D.; Fanwick, P. E.; Schelter, E. J.; Walensky, J. R.; Gagliardi, L.; Bart, S. C. Harnessing Redox Activity for the Formation of Uranium Tris(Imido) Compounds. *Nat. Chem.* **2014**, *6*, 919−926.
(28) Zi, G.; Jia, L.; Werkema, E. L.; Walter, M. D.; Gottfriedsen, J. P.; Andersen, R. A. Preparation and Reactions of Base-Free Bis(1,2,4-tri-*tert*-butylcyclopentadienyl)uranium Oxide, $Cp'_2UO$. *Organometallics* **2005**, *24*, 4251−4264.
(29) Zi, G.; Blosch, L. L.; Jia, L.; Andersen, R. A. Preparation and Reactions of Base-Free Bis(1,2,4-tri-*tert*-butylcyclopentadienyl)uranium Methylimide, $Cp'_2U$ = NMe, and Related Compounds. *Organometallics* **2005**, *24*, 4602−4612.
(30) Herasymchuk, K.; Chiang, L.; Hayes, C. E.; Brown, M. L.; Ovens, J.; Patrick, B. O.; Leznoff, D. B.; Storr, T. Synthesis and Electronic Structure Determination of Uranium(VI) Ligand Radical Complexes. *Dalton Trans* **2016**, *45*, 12576−12586.
(31) Bart, S. C.; Chlopek, K.; Bill, E.; Bouwkamp, M. W.; Lobkovsky, E.; Neese, F.; Wieghardt, K.; Chirik, P. J. Electronic Structure of Bis(Imino)Pyridine Iron Dichloride, Monochloride, and Neutral Ligand Complexes: A Combined Structural, Spectroscopic, and Computational Study. *J. Am. Chem. Soc.* **2006**, *128*, 13901−13912.
(32) Knijnenburg, Q.; Gambarotta, S.; Budzelaar, P. H. M. Ligand-Centred Reactivity in Diiminepyridine Complexes. *Dalton Trans.* **2006**, 5442−5448.
(33) Bill, E.; Bothe, E.; Chaudhuri, P.; Chlopek, K.; Herebian, D.; Kokatam, S.; Ray, K.; Weyhermüller, T.; Neese, F.; Wieghardt, K. Molecular and Electronic Structure of Four- and Five-Coordinate Cobalt Complexes Containing Two *o*-Phenylenediamine- or Two *o*-Aminophenol-Type Ligands at Various Oxidation Levels: An Experimental, Density Functional, and Correlated ab initio Study. *Chem. - Eur. J.* **2005**, *11*, 204−224.
(34) Kraft, S. J.; Williams, U. J.; Daly, S. R.; Schelter, E. J.; Kozimor, S. A.; Boland, K. S.; Kikkawa, J. M.; Forrest, W. P.; Christensen, C. N.; Schwarz, D. E.; Fanwick, P. E.; Clark, D. L.; Conradson, S. D.; Bart, S. C. Synthesis, Characterization, and Multielectron Reduction Chemistry of Uranium Supported by Redox-Active $\alpha$-Diimine Ligands. *Inorg. Chem.* **2011**, *50*, 9838−9848.
(35) Schelter, E. J.; Wu, R.; Scott, B. L.; Thompson, J. D.; Cantat, T.; John, K. D.; Batista, E. R.; Morris, D. E.; Kiplinger, J. L. Actinide Redox-Active Ligand Complexes: Reversible Intramolecular Electron-Transfer in $U(dpp\text{-}BIAN)_2/U(dpp\text{-}BIAN)_2(THF)$. *Inorg. Chem.* **2010**, *49*, 924−933.
(36) Vasudevan, K.; Cowley, A. H. Synthesis and Structures of 1,2-Bis(Imino)Acenaphthene (Bian) Lanthanide Complexes That Involve the Transfer of Zero, One, or Two Electrons. *Chem. Commun.* **2007**, 3464−3466.
(37) Cloke, F. G. N.; De Lemos, H. C.; Sameh, A. A. Homoleptic Diazadiene Complexes of Titanium, Yttrium, and Some Lanthanoid Elements. *J. Chem. Soc., Chem. Commun.* **1986**, 1344−1345.
(38) Recknagel, A.; Noltemeyer, M.; Edelmann, F. T. Organolanthanide(II) Chemistry. Reactions of $Cp^*_2Sm(THF)_2$ with 1,4-Diazadienes and Cyclooctatetraene. *J. Organomet. Chem.* **1991**, *410*, 53−61.
(39) Massarweh, G.; Dieter Fischer, R. Rearrangement of Tetrahydrofuran in Organolanthanides. The Crystal and Molecular Structures of Bis($\eta^5$-Cyclopentadienyl)Ytterbium(III)($\mu$-n-buten-2-olate) and Bis($\eta^5$-methylcyclopentadienyl)ytterbium(III) ($\mu$-$\eta^2$:$\eta^1$-tetrahydrofuran-2-olate). *J. Organomet. Chem.* **1993**, *444*, 67−74.
(40) Pangborn, A. B.; Giardello, M. A.; Grubbs, R. H.; Rosen, R. K.; Timmers, F. J. Safe and Convenient Procedure for Solvent Purification. *Organometallics* **1996**, *15*, 1518−1520.
(41) Ison, E. A.; Ison, A. Synthesis of Well-Defined Copper N-Heterocyclic Carbene Complexes and Their Use as Catalysts for a "Click Reaction": A Multistep Experiment That Emphasizes the Role of Catalysis in Green Chemistry. *J. Chem. Educ.* **2012**, *89*, 1575−1577.
(42) Schlosser, M.; Hartmann, J. Transmetalation and Double Metal Exchange: A Convenient Route to Organolithium Compounds of the Benzyl and Allyl Type. *Angew. Chem., Int. Ed. Engl.* **1973**, *12*, 508−509.
(43) Kiplinger, J. L.; Morris, D. E.; Scott, B. L.; Burns, C. J. Convenient Synthesis, Structure, and Reactivity of $(C_5Me_5)U(CH_2C_6H_5)_3$: A Simple Strategy for the Preparation of Monopentamethylcyclopentadienyl Uranium(IV) Complexes. *Organometallics* **2002**, *21*, 5978−5982.
(44) Bain, G. A.; Berry, J. F. Diamagnetic Corrections and Pascal's Constants. *J. Chem. Educ.* **2008**, *85*, 532.
(45) Buckley, B. R.; Neary, S. P. Thiadiazolidine 1-Oxide Systems for Phosphine-Free Palladium-Mediated Catalysis. *Tetrahedron* **2010**, *66*, 7988−7994.
(46) Schaub, T.; Radius, U. A Diazabutadiene Stabilized Nickel(0) Cyclooctadiene Complex: Synthesis, Characterization and the Reaction with Diphenylacetylene. *Z. Anorg. Allg. Chem.* **2006**, *632*, 807−813.
(47) Martins, R. S.; Filgueiras, C. L.; Visentin, L. d. C.; Bordinhao, J.; Ferreira, L. C. 2,3-Bis(2-Ethylphenylimino)Butane. *Acta Crystallogr., Sect. E: Struct. Rep. Online* **2007**, *63*, o4544.
(48) Gonsalvi, L.; Gaunt, J. A.; Adams, H.; Castro, A.; Sunley, G. J.; Haynes, A. Quantifying Steric Effects of $\alpha$-Diimine Ligands. Oxidative Addition of MeI to Rhodium(I) and Migratory Insertion in Rhodium(III) Complexes. *Organometallics* **2003**, *22*, 1047−1054.
(49) Cope-Eatough, E. K.; Mair, F. S.; Pritchard, R. G.; Warren, J. E.; Woods, R. J. Palladium Co-ordination Chemistry of $\beta$-Diimines: A Preparative and Structural Comparison with $\alpha$-Diimines. *Polyhedron* **2003**, *22*, 1447−1454.
(50) Jantunen, K. C.; Burns, C. J.; Castro-Rodriguez, I.; Da Re, R. E.; Golden, J. T.; Morris, D. E.; Scott, B. L.; Taw, F. L.; Kiplinger, J. L. Thorium(IV) and Uranium(IV) Ketimide Complexes Prepared by Nitrile Insertion into Actinide-Alkyl and -Aryl Bonds. *Organometallics* **2004**, *23*, 4682−4692.
(51) Marks, T. J. *Prog. Inorg. Chem.*; John Wiley & Sons: New York, 1979; Vol. 25.
(52) Lam, O. P.; Anthon, C.; Heinemann, F. W.; O'Connor, J. M.; Meyer, K. Structural and Spectroscopic Characterization of a Charge-Separated Uranium Benzophenone Ketyl Radical Complex. *J. Am. Chem. Soc.* **2008**, *130*, 6567−6576.
(53) Anderson, N. H.; Yin, H.; Kiernicki, J. J.; Fanwick, P. E.; Schelter, E. J.; Bart, S. C. Investigation of Uranium Tris(Imido) Complexes: Synthesis, Characterization, and Reduction Chemistry of $[U(NDIPP)_3(THF)_3]$. *Angew. Chem., Int. Ed.* **2015**, *54*, 9386−9389.
(54) Smith, A. L.; Martin, P.; Prieur, D.; Scheinost, A. C.; Raison, P. E.; Cheetham, A. K.; Konings, R. J. M. Structural Properties and Charge Distribution of the Sodium Uranium, Neptunium, and Plutonium Ternary Oxides: A Combined X-Ray Diffraction and XANES Study. *Inorg. Chem.* **2016**, *55*, 1569−1579.

(55) Kosog, B.; La Pierre, H. S.; Denecke, M. A.; Heinemann, F. W.; Meyer, K. Oxidation State Delineation via U $L_{III}$-Edge XANES in a Series of Isostructural Uranium Coordination Complexes. *Inorg. Chem.* **2012**, *51*, 7940−7944.
(56) Den Auwer, C.; Simoni, E.; Conradson, S.; Madic, C. Investigating Actinyl Oxo Cations by X-Ray Absorption Spectroscopy. *Eur. J. Inorg. Chem.* **2003**, *2003*, 3843−3859.
(57) Vlaisavljevich, B.; Diaconescu, P. L.; Lukens, W. L., Jr.; Gagliardi, L.; Cummins, C. C. Investigations of the Electronic Structure of Arene-Bridged Diuranium Complexes. *Organometallics* **2013**, *32*, 1341−1352.
(58) Brendebach, B.; Banik, N. L.; Marquardt, C. M.; Rothe, J.; Denecke, M.; Geckeis, H. X-Ray Absorption Spectroscopic Study of Trivalent and Tetravalent Actinides in Solution at Varying pH Values. *Radiochim. Acta* **2009**, *97*, 701.
(59) Chiang, M.-H.; Williams, C. W.; Soderholm, L.; Antonio, M. R. Coordination of Actinide Ions in Wells−Dawson Heteropolyoxoanion Complexes. *Eur. J. Inorg. Chem.* **2003**, *2003*, 2663−2669.
(60) Lukens, W. W., Jr.; Allen, P. G.; Bucher, J. J.; Edelstein, N. M.; Hudson, E. A.; Shuh, D. K.; Reich, T.; Andersen, R. A. Structures of Substituted-Cyclopentadienyl Uranium(III) Dimers and Related Uranium Metallocenes Deduced by EXAFS. *Organometallics* **1999**, *18*, 1253−1258.
(61) Budzelaar, P. H. M.; de Bruin, B.; Gal, A. W.; Wieghardt, K.; van Lenthe, J. H. Metal-to-Ligand Electron Transfer in Diiminopyridine Complexes of Mn-Zn. A Theoretical Study. *Inorg. Chem.* **2001**, *40*, 4649−4655.
(62) De Bruin, B.; Peters, T. P. J.; Thewissen, S.; Blok, A. N. J.; Wilting, J. B. M.; De Gelder, R.; Smits, J. M. M.; Gal, A. W. Dioxygen Activation by a Mononuclear $Ir^{II}$-Ethene Complex. *Angew. Chem., Int. Ed.* **2002**, *41*, 2135−2138.
(63) Kindra, D. R.; Evans, W. J. Magnetic Susceptibility of Uranium Complexes. *Chem. Rev.* **2014**, *114*, 8865−8882.
(64) Schelter, E. J.; Yang, P.; Scott, B. L.; Thompson, J. D.; Martin, R. L.; Hay, P. J.; Morris, D. E.; Kiplinger, J. L. Systematic Studies of Early Actinide Complexes: Uranium(IV) Fluoroketimides. *Inorg. Chem.* **2007**, *46*, 7477−7488.
(65) Newell, B. S.; Rappe, A. K.; Shores, M. P. Experimental Evidence for Magnetic Exchange in Di- and Trinuclear Uranium(IV) Ethynylbenzene Complexes. *Inorg. Chem.* **2010**, *49*, 1595−1606.
(66) Kozimor, S. A.; Bartlett, B. M.; Rinehart, J. D.; Long, J. R. Magnetic Exchange Coupling in Chloride-Bridged 5f−3d Heterometallic Complexes Generated via Insertion into a Uranium(IV) Dimethylpyrazolate Dimer. *J. Am. Chem. Soc.* **2007**, *129*, 10672−10674.